Plasma Sci. Technol. **26** (2024) 094010 (12pp) https://doi.org/10.1088/2058-6272/ad6815

Synthesis of NO by rotating sliding arc discharge reactor with conical-spiral electrodes

Bingyan CHEN (陈秉岩)[1,2,*], **Qi LIU** (刘琦)[2], **Xu LI** (李旭)[2], **Chunyang ZHANG** (张春阳)[3], **Xiangbin GUO** (郭湘彬)[2], **Qingzhou YU** (余青洲)[4], **Zhicheng TANG** (唐志承)[2], **Xiang HE** (何湘)[1], **Wei SU** (苏巍)[1] **and Yongfeng JIANG** (蒋永锋)[3,*]

[1] College of Mechanics and Engineering Science, Hohai University, Nanjing 211100, People's Republic of China
[2] College of Mechanical and Electrical Engineering, Hohai University, Changzhou 213200, People's Republic of China
[3] College of Materials Science and Engineering, Hohai University, Changzhou 213200, People's Republic of China
[4] College of Information Science and Engineering, Hohai University, Changzhou 213200, People's Republic of China

[*]E-mail of corresponding authors: byan@foxmail.com and 20051700@hhu.edu.cn

Received 26 February 2024, revised 25 July 2024
Accepted for publication 26 July 2024
Published 30 August 2024

Abstract

The present work investigates the potential applications of nitrogen oxides (NO_x), particularly nitric oxide (NO) and nitrogen dioxide (NO_2), generated through discharge plasma in diverse sectors such as medicine, nitrogen fixation, energy, and environmental protection. In this study, a rotating sliding arc discharge reactor was initially employed to produce high concentrations of gaseous NO_x, followed by the utilization of a molybdenum wire redox reactor for NO_2-to-NO conversion. The outcomes reveal that the discharge states and generations of NO_x are affected by varying parameters, including the applied energies, frequencies and airflow states (1.3–2.6 m/s are the laminar flow, 2.6–5.2 m/s are the transition state, 5.2–6.5 m/s are the turbulent flow), and the concentrations of NO_x within the arc discharge are higher than that in the spark discharge. Moreover, the concentrations of NO, NO_2 and NO_x gradually increased, and the concentration ratios of NO/NO_2 and NO_x/NO_2 decreased with increasing the applied energy for one cycle from 14.8 mJ to 24.3 mJ. Meanwhile, the concentrations of NO, NO_2 and NO_x gradually decreased, and the concentration ratios of NO/NO_2 and NO_x/NO_2 first decreased and then increased with increasing the applied frequencies from 5.0 kHz to 9.0 kHz. Further, the concentrations of NO, NO_2 and NO_x gradually decreased, and the concentration ratios of NO/NO_2 and NO_x/NO_2 first increased and then decreased with increasing the air flow speeds from 1.3 m/s to 6.5 m/s. Lastly, the concentrations of NO increased and NO_2 decreased with increasing temperature from 25 °C to 400 °C using molybdenum converted. These findings provide experimental support for the application of plasma in the fields of medicine, nitrogen fixation, energy and environmental protection.

Keywords: rotating sliding arc discharge, NO_x, synthesis of NO, redox reaction

(Some figures may appear in colour only in the online journal)

[*] Authors to whom any correspondence should be addressed.

1. Introduction

Nitric oxide (NO) has long been recognized as an atmospheric pollutant that is harmful to humans and the environment. However, medical research has found that NO is actually an endogenous gas molecule present in the human body, and that inhalation of low concentrations of NO (3–20 ppm) can be an effective treatment for acute respiratory failure, pulmonary arterial hypertension, and many other lung-related disorders [1–6]. Meanwhile, many chronic diseases lead to a decrease in the endogenous production of NO in the organism, so inhalation therapy of NO has emerged, and methods of NO synthesis are increasingly being emphasized.

Currently employed medical-grade NO is obtained by diluting bottles of highly concentrated NO gas containing a nitrogen (N_2) carrier gas [7, 8]. Industrially, manufacturers mainly prepare NO by reacting sodium nitrite ($NaNO_2$) with dilute sulfuric acid (H_2SO_4), which is a complicated and expensive process. The commonly used methods of NO synthesis by high voltage discharge are pulsed arc discharge, pulsed spark discharge, corona discharge, etc. Hu *et al* [9] studied pulsed arc discharge to synthesize NO, and investigated the effect of discharging with a needle-plate electrode on the concentration of NO, with the aim of finding the optimal parameters for synthesizing NO. Yu *et al* [10] used pulsed spark discharge to investigate two types of NO generators: an off-line NO generator and an on-line NO generator placed directly inside the suction line. The aim was to develop a lightweight, portable device that could be used for bedside or portable use. Huang *et al* [11] used AC arc discharge to generate NO and removed excess NO_2 with ammonium sulfite ($(NH_4)_2SO_3$) solution as a way to develop an efficient and cost-effective on-site power generation system. These discharge synthesis methods for NO are mainly characterized by their low price but low NO concentration and small gas flow rate, which are ideal for immediate use and not suitable for mass production. A pressing need exists for a cost-effective, scalable NO production technique.

This study delves into the sliding arc discharge technique of a conical spiral electrode that can produce high NO concentration and high gas flow rate, and systematically investigates the effects of gas flow speed, applied energy and applied frequency on the discharge state and the concentrations of NO, NO_2, and NO_x. The relationship between NO and NO_2 is also explored. Additionally, we study the effects of air flow speed, applied energy and applied frequency on the relative spectral intensities of the rotating sliding arc discharge. Finally, the molybdenum wire temperature was adjusted to minimize NO_2 while increasing NO production by taking advantage of the property that the molybdenum wire can convert excess NO_2 to NO at high temperatures. This experiment can contribute to NO synthesis research.

2. Experimental setup and method

2.1. Apparatus

Figure 1 presents the NO synthesis system, and figure 1(a) shows the rotational sliding arc discharge synthesis system

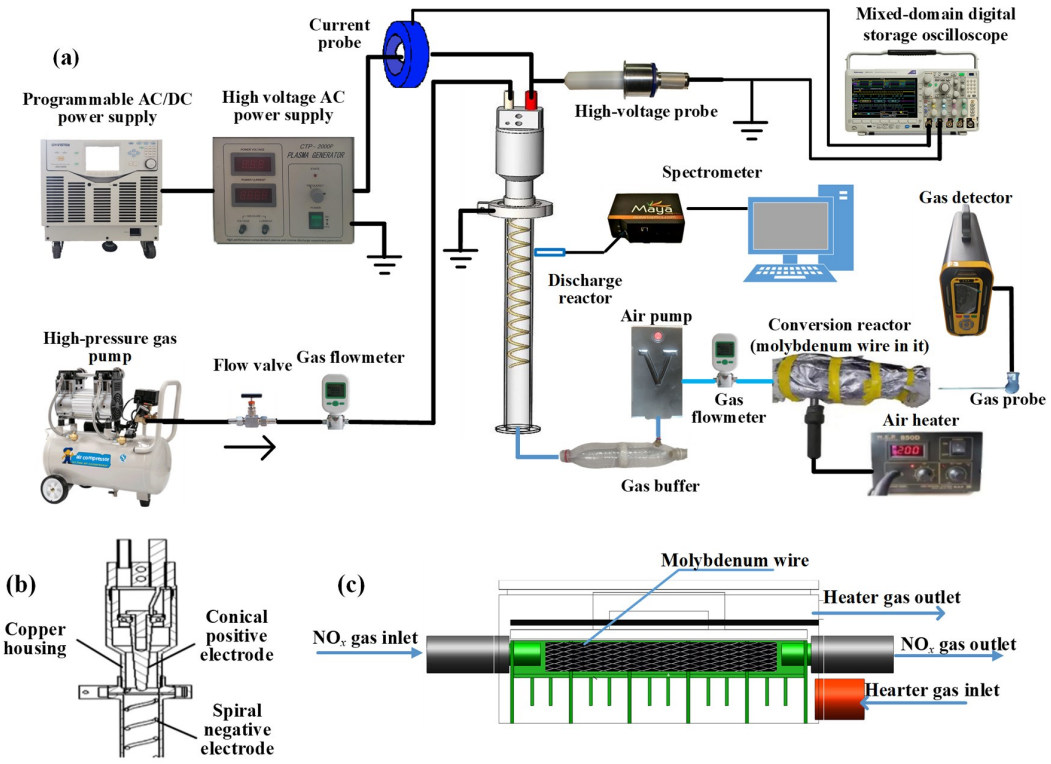

Figure 1. Draft of rotating sliding arc discharge synthesized NO. (a) Discharge system, (b) reactor structure, (c) molybdenum wire converter.

for NO, which includes a conical-spiral sliding arc reactor, high-voltage AC power supply, power supply parameter detection system, high-temperature molybdenum wire conversion system, gas detection system, and spectral detection system. Figure 1(b) shows the structure of the discharge reactor, and figure 1(c) shows the conversion reactor for NO_2 to NO.

Gas supplied by a high-pressure gas pump passes through a gas flow meter to reach the sliding arc reactor, where it flows into a gas buffer bottle after a high-pressure discharge.

To maintain a constant for the flow field state in the discharge area, this gas buffer bottle has equally large holes at both ends, and then a pump draws low-flow gas from the gas buffer into the molybdenum wire converter for NO_2 converted to NO, and the concentrations of NO are analyzed at the tail end. The molybdenum wire converter is designed based on the property that molybdenum wire can convert NO_2 into NO under high temperature. High-temperature gas is blown into the conversion device by a hot air gun to heat the molybdenum wire, the heat gas temperature can be adjustable from 0 °C to 500 °C.

The cone-spiral rotating sliding arc reactor consisted of a cyclone ring, a conical inner electrode, a spiral ground electrode, a cylindrical shell made of copper, and a quartz tube.

The air supplied by the air pump navigates through the cyclone circle to form a spiral airflow, which pushes the arc to move along the lower spiral grounding electrode, thus establishing a steady plasma torch.

The conical inner electrode is made of high-temperature resistant 2080 stainless steel, and the spiral grounding electrode is made of titanium, with an outer diameter and length of 20.0 mm and 150.0 mm, respectively, and the cyclone ring is a ring with 8 holes of 2.5 mm in diameter, 28.0 mm in diameter, and the angle of the axis is 45°.

In addition, the plasma excitation power supply was a power density modulation (PDM) high-voltage AC power supply (Corona Lab, CTP-2000P) and a programmable AC/DC power supply (GW Instek, GPK-2302) was used to regulate the applied voltage. A mixed-domain digital storage oscilloscope (Tektronix, MDO3054B) equipped with a high-voltage probe (North Star, PVM-5) and a current probe (Pearson, 6595) was used to measure applied voltages and currents loaded on the rotating sliding arc discharge reactor. A NO_x detector (Jishunan, JK90-M4-GD) was used to detect the NO_x concentration and a fiber optic spectrometer (Ocean Optics, Maya 2000Pro) was used to detect the relative spectral intensity of the discharge.

2.2. Formation principles of NO

In the process of atmospheric pressure high-voltage discharge generating plasma, significant byproducts including ultraviolet radiation, shockwaves, energetic electrons, and reactive free radicals coexist. The presence of these reactive species is fundamental to the practical exploitation of plasma technology.

In discharges using air as the gas source, the gas between the electrodes is broken down to form plasma filaments. Within the discharge region, there are numerous free electrons, positive and negative ions, as well as excited-state atoms or gas molecules.

Collisions and interactions among reactive components result in the conversion of particle kinetic energy into the internal energy of the collided particles, leading to the excitation, dissociation, or ionization of more particles. Chemical reactions or conversions occur among reactive components, forming gaseous products such as NO, NO_2, and O_3. This study centers on the methodology of NO synthesis via rotary sliding arc discharge, where N_2 and O_2 in the air are excited and ionized within the discharge zone, as described by the following reaction [12, 13]:

$$e + O_2 \rightarrow O + O + e \tag{1}$$

$$e + N_2 \rightarrow N + N + e \tag{2}$$

$$e + N_2 \rightarrow N_2^* + e \tag{3}$$

When thermal carrier molecules M are involved, the reaction between O radicals and O_2 molecules results in the formation of O_3. The reaction process is as follows [14–16]:

$$O + O_2 + M \rightarrow O_3 + M \tag{4}$$

Excited-state oxygen atoms (O) react with N_2 to form NO and N radicals. The reaction process is as follows [12, 13, 17]:

$$O + N_2 \rightarrow NO + N \tag{5}$$

$$N + O_2 \rightarrow NO + O \tag{6}$$

In air discharge, another product is NO_2, which originates from the oxidation of NO. NO is easily oxidized by O_3 and O to form NO_2. The reaction process is as follows [18, 19]:

$$NO + O_3 \rightarrow NO_2 + O_2 \tag{7}$$

$$NO + O + M \rightarrow NO_2 + M \tag{8}$$

When the thermal plasma temperature generated by arc discharge is below 3800 K, O_2 reacts with NO, and free radical O reacts with N_2, producing small amounts of NO_2 and N_2O. The reaction process is as follows [9]:

$$NO + NO + O_2 \rightarrow 2NO_2 \tag{9}$$

$$N_2 + O \rightarrow N_2O \tag{10}$$

2.3. Applied energy analysis

The electrical characteristics of a rotary sliding arc discharge

can be characterized by measuring the applied voltage and current. The calculation of applied energy (E) can be obtained by integrating the product of voltage and current with respect to time t [20–22].

$$E = \int_0^T u(t)i(t)\mathrm{d}(t), \tag{11}$$

here, $u(t)$ and $i(t)$ respectively represent the voltage function and current function in the discharge circuit. In typical scenarios, $u(t)$ and $i(t)$ represent complex functions of time. Therefore, the full width at half maximum (FWHM) method is employed to calculate the energy of sliding arc discharge. The calculation formula is as follows [23, 24]:

$$P_\mathrm{r} = E_\mathrm{d} \cdot f_\mathrm{d}, \tag{12}$$

here, P_r represents the total energy (J) consumed by the reactor when the time is 1 s, E_d represents the energy (mJ) consumed by the reactor in one applied energy cycle, and f_d represents the frequency.

The applied energy (E_d) is the sum of the energies of two power peaks. The calculation formula is as follows [23]:

$$E_\mathrm{d} = P_1 t_1 + P_2 t_2, \tag{13}$$

here, P_1 represents the peak power (mJ) of the first half of the applied energy cycle, P_2 represents the peak power (mJ) of the second half of the applied energy cycle, t_1 and t_2 represent the respective time durations (μs) of the energy half-peak values.

Figure 2 shows the typical waveforms of the applied voltage and current loaded on the discharge electrodes, the experiment conditions were with the applied frequency as 7.0 kHz and the air flow speed as 1.3 m/s. Therefore, E_d is 14.89 mJ and P_r is 104.23 W.

Due to the variation in experimental parameters in sliding arc discharge, secondary peaks in the voltage and current waveforms may occur, leading to the changes in the energy waveform.

As shown in figure 3, the applied frequency is 7.0 kHz, the air flow speed is 2.6 m/s. When calculating the energy, the valley at the half applied energy cycle was taken as the division point and the half cycle was divided into two parts. The energy of the half cycle can be obtained by adding the two parts of the energy.

When the sliding arc discharge is converted to spark discharge, the half-peak full-width method can also be employed to calculate. As shown in figure 4, the applied frequency is 7.0 kHz and the air flow speed is 5.2 m/s. The power spectral line shown in figure 4(c) is a triangular energy peak, and the half-peak full-width method is used to calculate the energy spectrum to get the energy of single

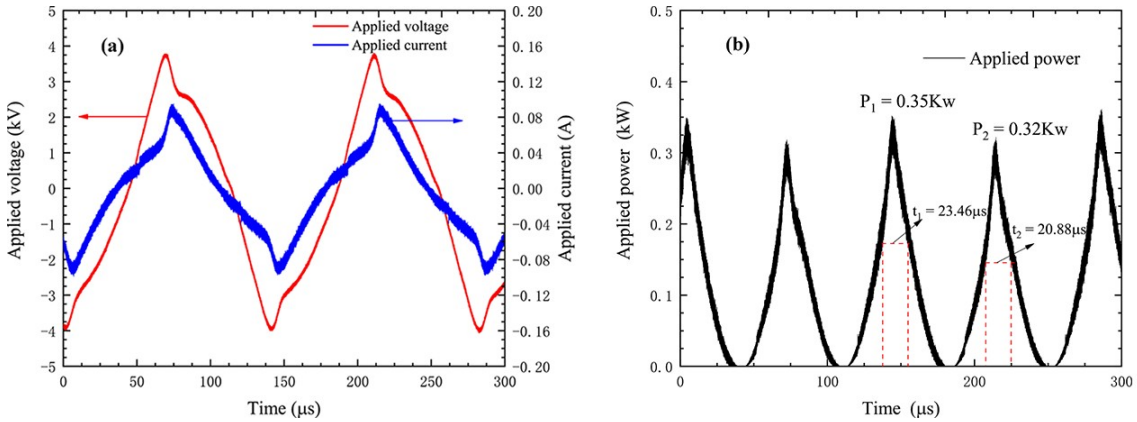

Figure 2. Waveforms loaded on the discharge reactor under applied frequency of 7.0 kHz and air flow speed of 1.3 m/s. (a) Applied voltage and current, (b) applied power.

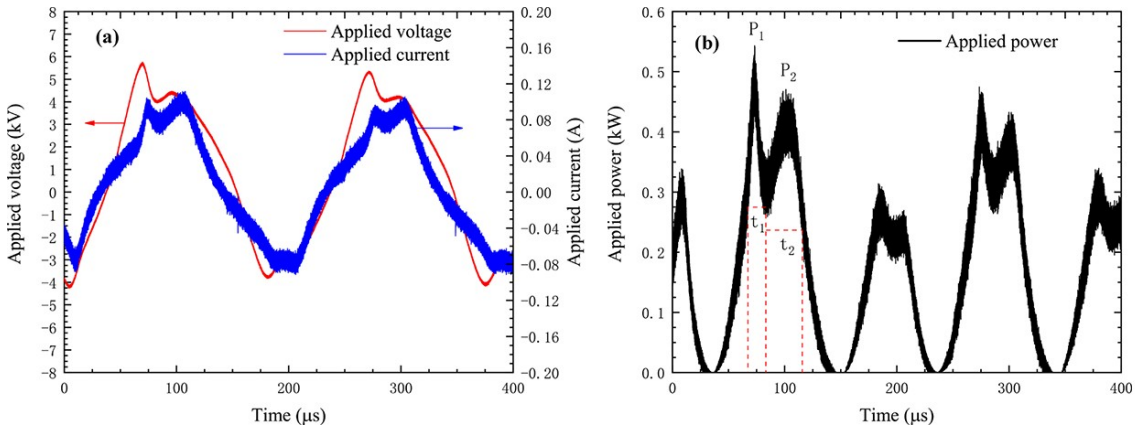

Figure 3. Waveforms loaded on the discharge reactor under applied frequency of 7.0 kHz and air flow speed of 2.6 m/s. (a) Applied voltage and current, (b) applied power.

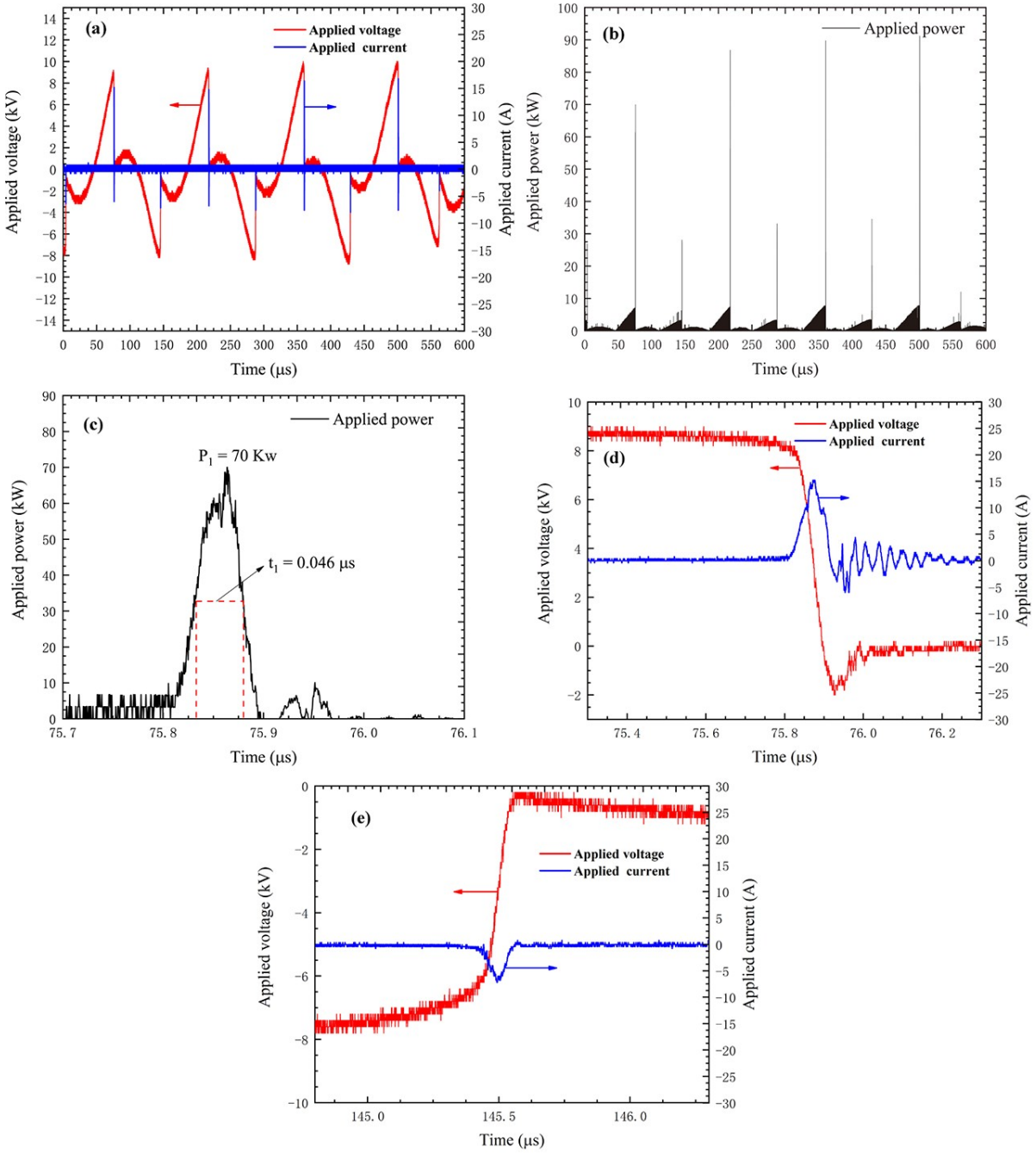

Figure 4. Waveforms loaded on the discharge reactor. (a) Applied voltage and current waveforms, (b) applied power waveform, (c) power waveform at the instant of discharge, (d) positive breakdown, (e) negative breakdown.

applied energy cycle. Figures 4(d) and (e) depict instantaneous positive and negative breakdowns; brief high-voltage breakdowns trigger significant currents, swiftly lowering electrode voltage, recurrently interrupting discharge, sustaining spark condition.

2.4. Fluid flow state judgment

To investigate the influence of fluid flow state on sliding arc discharge, the Reynolds number (*Re*) of fluid flow needs to be calculated. *Re* is a dimensionless quantity that characterizes the state of fluid flow, and it is the ratio of inertial force and viscous force of the fluid. In fluid mechanics, *Re* is often used to distinguish the state of fluid flow. When $Re < 2320$, the flow state is laminar; when $2320 < Re < 4000$, the flow state is laminar and turbulent transition state, mainly turbulent; when $Re > 4000$, the flow state is turbulent. The formula of *Re* is as follows:

$$Re = \frac{\upsilon d}{v} = \frac{\rho \upsilon d}{\mu}, \tag{14}$$

where υ is the fluid flow rate (m/s), d is the characteristic length (m); v is the kinematic viscosity of air. p is the fluid density (m^3/kg). μ is the dynamic viscosity (kg/(m·s)).

At a pressure of 101.3 kPa and a temperature of 20 °C,

the air dynamic viscosity measures 14.8×10^{-6} m^2/s. The fluid flow rate is calculated by the following formula:

$$u = \frac{4Q}{\pi(D_1^{\,2} - d_1^{\,2})}, \tag{15}$$

where Q is the fluid flow rate (m^3/s), D_1 is the diameter of the fluid channel (inner diameter of the helical electrode) in the plasma region of action (m); and d_1 is the diameter of the cone electrode.

The gas flow rate in the discharge reactor corresponds to the gas flow speed and the flow state, as shown in table 1. The gas flow states are laminar, transition of laminar and turbulent, and turbulent when the gas flow speeds are less than 2.6 m/s, from 2.6 m/s to 5.2 m/s, and more than 5.2 m/s, respectively.

Table 1. Gas flow rate in the discharge reactor corresponding to the gas flow speed and flow state.

Gas flow rate (L/min)	Gas flow speed (m/s)	Kinematic viscosity ($\times10^6$ m^2/s)	*Re*	Flow state
20	1.3	28.95	905.11	Laminar
40	2.6	26.65	1966.22	Laminar
60	3.9	23.54	3339.36	Transition
80	5.2	21.83	4801.03	Turbulent
100	6.5	20.50	6389.38	Turbulent

3. Results and discussion

3.1. Influence of gas flow speed

In order to investigate the effect of gas flow speed on the discharge state of sliding arc discharge and on the concentration of NO, NO_2 and NO_x, the gas flow speed was adjusted by a high-pressure gas pump, and the waveforms of the applied voltage and current, the concentration of NO_x, and the relative intensity of discharge emission spectra were measured. The experimental conditions were as follows: the applied voltage loaded on the reactor was 4.0–11.0 kV, the applied frequency was 7.0 kHz, and the gas flow speeds were varied from 1.3 m/s to 6.5 m/s.

Figures 5 and 6 show the discharge states, discharge spectra and NO_x. It was obtained that when the gas flow speed increased, the sliding arc discharge was transformed from arc discharge to spark discharge, meanwhile, the concentrations of NO, NO_2 and NO_x decreased while the relative intensity of discharge emission spectra increased.

Figures 5(a)–(c) show the waveforms of applied voltage and applied current at different gas flow speeds. When the gas flow speed is 1.3 m/s, the discharge state is arc discharge. When the gas flow speed is increased, the discharge states change from arc to spark. When the gas flow speed reaches 3.9 m/s, the discharge state is in the transition state of arc and spark. As the gas flow speed increased to 5.2 m/s, the discharge state is completely transformed into the spark discharge. The breakdown and extinction processes occur frequently in the discharge region. At the moment of breakdown, a discharge channel is formed between the electrodes, the applied current increases rapidly while the applied voltage decreases rapidly, and then the applied current returns to zero after some small cycles of small oscillations.

The findings can be characterized as follows. When the gas flow speed is 1.3 m/s, the gas flow state is laminar, and the flow direction of gas flow is basically the same. During

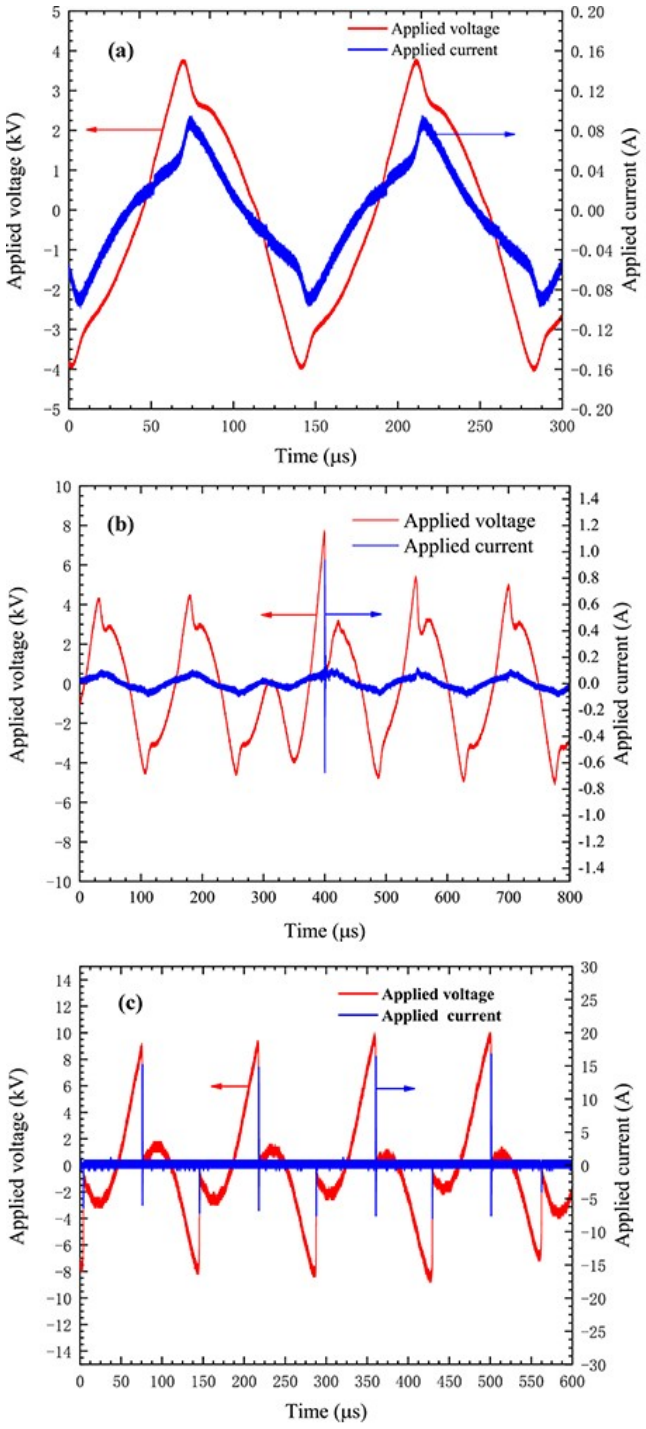

Figure 5. The waveforms of applied voltage and current at different gas flow speeds. (a) Arc with gas flow speed of 1.3 m/s, (b) transition state with gas flow speed of 3.9 m/s, (c) spark with gas flow speed of 5.2 m/s.

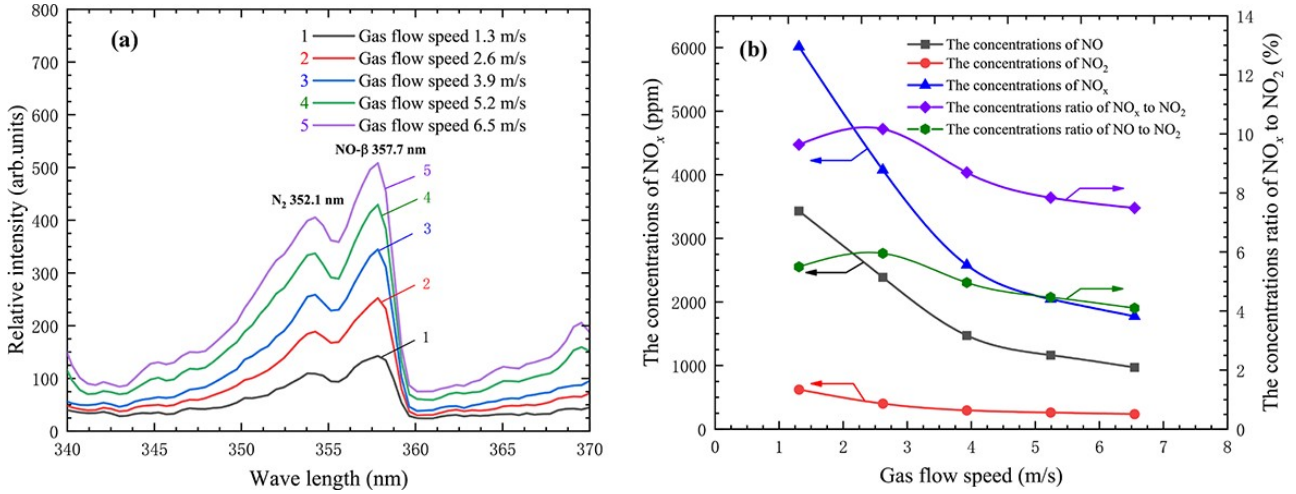

Figure 6. The intensities of discharge spectra and concentrations of NO_x with different gas flow speeds. (a) The discharge emission spectral intensity, (b) the concentrations and the ratios of NO, NO_2 and NO.

the discharge process, the energy provided by the power supply is sufficient to maintain the continuous existence of the arc due to the limited diffusion of ions or electrons in the arc channel [25−27].

The transition mode of laminar and turbulent affects the discharge state from two aspects: (1) the drift diffusion of charged particles between electrodes is accelerated, thus reducing the density of electrons and ions in the discharge region, which makes the distribution of charged particles in the discharge region more uniform and increases the area of the plasma plume; (2) the convective heat transfer between the plasma plume and the air increases, reducing the temperature of the discharge area, which leads to increased energy dissipation during the discharge process. When the energy provided by the power supply is not enough to maintain the arc channel, the discharge mode is transformed into spark discharge. Therefore, laminar flow is in the transition mode of arc and spark. Turbulent vortices in turbulent mode are more likely to penetrate the plasma plume and increase the heat and mass exchange between the plasma plume and the flowing air, thus aggravating the dissipation of arc energy [28]. Therefore, the discharge mode in turbulent mode is spark discharge.

Figure 6 shows the relative intensities of the discharge spectra and the concentrations of NO, NO_2 and NO_x at different gas flow speeds. When the gas flow speed is low to 1.3 m/s, the relative intensity of spectra is rather low but the concentrations of NO, NO_2 and NO_x are quite large. When the gas flow speeds increased, the relative intensities increased, and the concentrations of NO, NO_2 and NO_x decreased. When the gas flow speed increased to 6.5 m/s, the relative intensities of the discharge emission spectra increase to the largest, while the concentrations of NO, NO_2 and NO_x decrease to the lowest.

The discharge emission spectral intensity increases when the gas flow speed increases. This is because low gas flow speed (0–2.6 m/s) is in a laminar state and is characterized as arc discharge. Arc discharge is primarily dominated by electron excitation, the discharge region increases with the increase of airflow speeds, resulting in an increase in the intensities of discharge emission spectra. As the gas flow speed increases from 2.6 m/s to 6.5 m/s, the gas flow is in a transition and turbulent state and the discharge state is characterized as transition and spark discharge. The plasma plume along the sliding region of the spiral electrode increases, leading to more particles being ionized, so that discharge emission spectral intensity increases.

The concentrations of NO_x decline with escalating gas flow speed. This phenomenon can be attributed to two factors. Firstly, despite an increased gas volume, the rate of discharge reactions exhibits minimal variation, thereby contributing to the decrease. Secondly, as the speed rises, the discharge shifts from arc to spark mode, altering the process from predominantly electron excitation to a blend of electron excitation and ionization via collisions. Spark discharges generate ultraviolet radiation and energetic electron interactions, effectively breaking down or transforming reaction intermediates, ultimately resulting in a lower NO_x concentration at higher flow rates [29–31].

When the gas flow speeds increased, the concentration ratios of NO_x (NO) to NO_2 initially rose and then fell. The reason would be related by the relationships between the discharge states and air flow states in the discharge reactor (see figure 5). When the gas flow state is laminar, the discharge state is arc discharge and has a higher local thermodynamic temperature in the discharge reactor. It has a higher reaction rate for NO reacted with O_2 and converted to NO_2 under high temperature. When the gas flow state is transition, the discharge state is the transition state between arc and spark discharge. The spark discharge channels have higher transient temperatures (above 2000 K). This will help improve the rate of N_2 reacting with O_2 to generate NO [31–33]. It is a complete spark discharge when the gas state is turbulent, and the discharge intensity decreases with the increase of gas flow rate, and the generated active components such as NO also decrease.

Hence, the concentration ratios of NO_x (NO) to NO_2 have the trend of initially increased and then decreased with

the increasing gas flow speed. This observation provides a reference for the practical application value of optimizing the gas flow speed range.

3.2. Influence of applied energy

In order to investigate the discharge states and NO_x generations affected by the applied energies loaded on the sliding arc discharge reactor, the applied energy was adjusted by the input voltage. The experimental conditions are as follows: the applied frequency is 7.0 kHz, the gas flow speed is 2.3 m/s (the gas flow state is laminar, as seen in table 1), and the applied energy is increased from 14.8 mJ to 24.3 mJ per discharge term. Figures 7 and 8 show the discharge states, the discharge spectra and the concentrations of NO_x under different applied energies. It was obtained that when the applied energy increased, the sliding arc discharge state was transformed from spark discharge to arc discharge, and the concentrations of NO, NO_2 and NO_x increased while the relative intensity of the discharge emission spectra decreased.

Figure 7 shows the waveforms of applied voltage and applied current at various applied energies. When the applied energy is low (from 14.8 mJ to 17.2 mJ), the discharge state is spark. When the applied energy for one cycle (from 17.2 mJ to 19.6 mJ) is increased, the discharge is in the transition state of spark and arc. When the applied energy for one cycle is increased to more than 19.6 mJ, the discharge state is arc.

The results can be explained as follows. With low applied energy, the momentary high-voltage breakdown generates a large current, which instantaneously pulls down the voltage between the electrodes. What is more, the energy provided by the power supply is not enough to maintain the energy dissipation caused by the discharge, causing the discharge to be interrupted repeatedly and thus maintaining a spark state. Conversely, when the applied energy is higher, it is sufficient to maintain the energy dissipation caused by the discharge, so that it is possible to sustain a larger voltage and current between the high-voltage electrodes during the discharge, maintaining an arc state. When the applied energy is neither too low nor too high, at a certain value, the discharge resides in a transitional state between spark and arc.

Figure 8(a) shows the relative intensity of discharge spectra at different applied energies. The relative spectral intensities from discharge region are very intensive when the applied energy is less than 17.2 mJ. However, the concentrations of NO, NO_2 and NO_x are rather low. When the applied energy is increased, the relative intensities decrease, but the concentrations of NO, NO_2 and NO_x increase. As the applied energies continue increasing to 24.3 mJ, the relative intensities decreased, and the concentrations of NO, NO_2 and NO_x increased.

Indeed, during the spark discharge phase, a high electric field is maintained between the electrodes before the breakdown, and charged particles within the discharge channel is attained higher energy during the breakdown event [23].

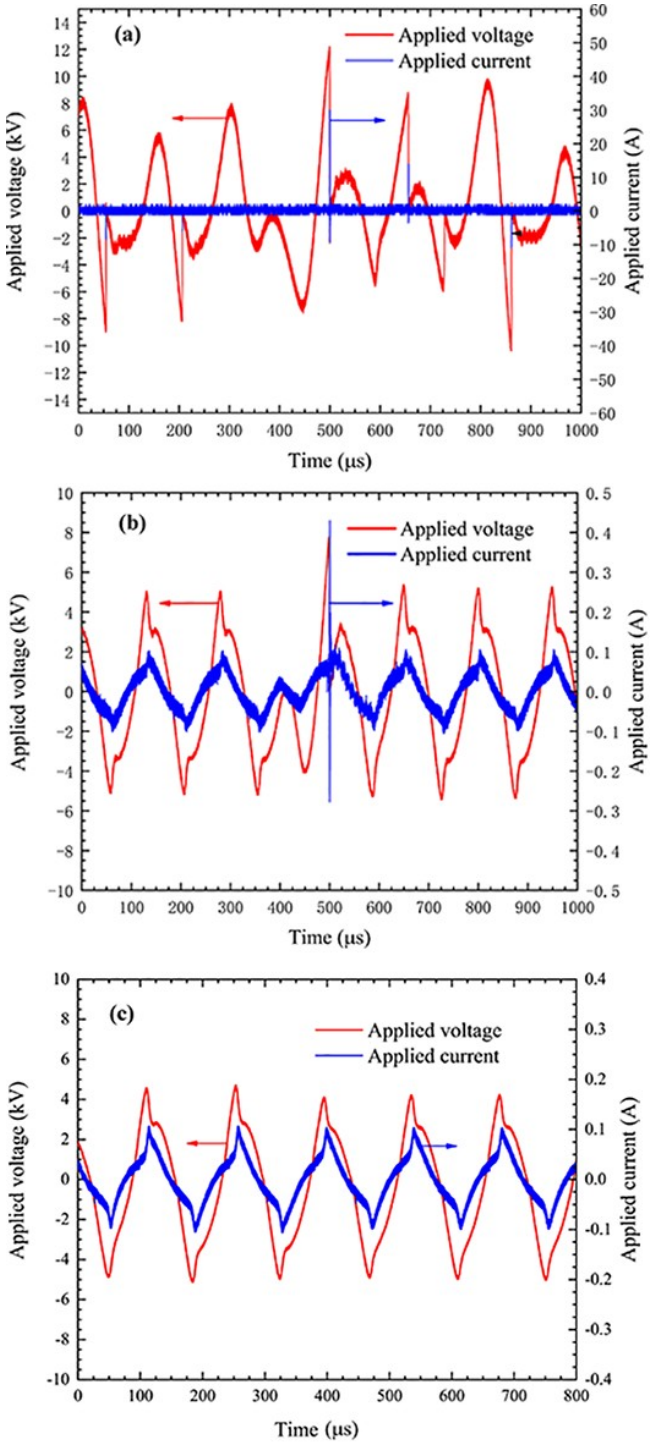

Figure 7. Waveforms of voltage and current at different applied energies. (a) Spark discharge under 14.8 mJ, (b) transition state between spark and arc under 17.2 mJ, (c) arc discharge under 19.6 mJ.

Hereby, the relative spectra intensities from the spark discharge are stronger than those from arc discharge, and the generation of NO is easier exiting in the discharge region. Consequently, this results in a more intense discharge relative intensity for NO.

As the applied energy rises, the density of charged particles increased in the discharge region, thus augmenting the production of NO_x. In the regime of spark discharge mode,

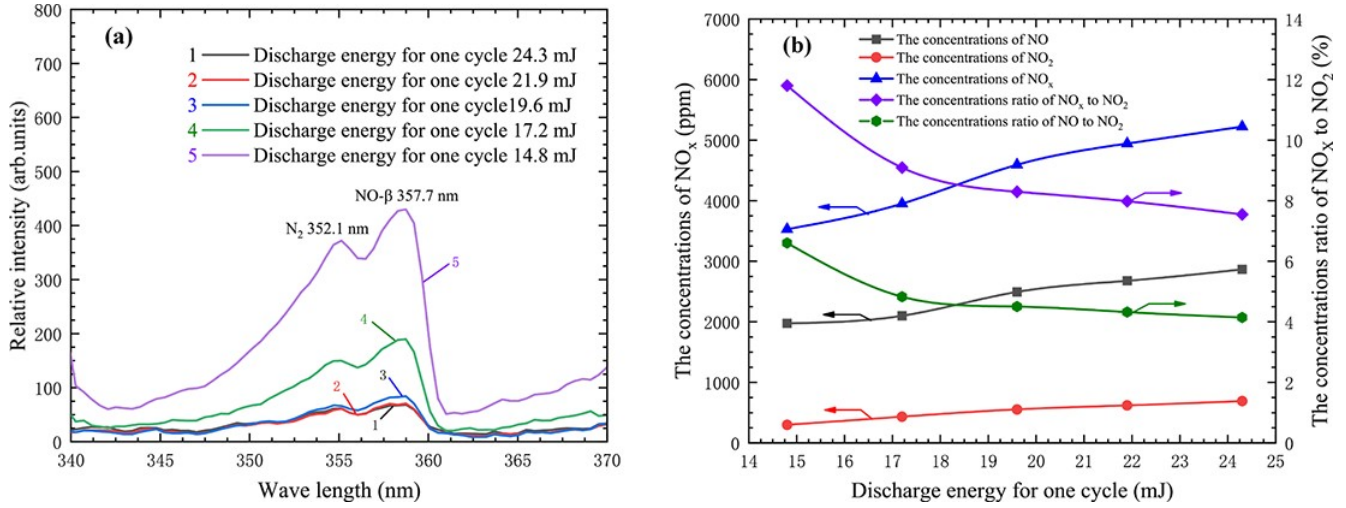

Figure 8. The relative intensities and the concentrations of NO_x under different applied energies. (a) The relative intensity, (b) the concentrations and the ratios of NO, NO_2 and NO_x.

characterized by lower supplied powers, while the conditions are favorable for the production of NO, the brevity of the discharge event results in the concentration of NO being maintained at comparatively modest levels.

When the discharge stages are during the spark or transition state between spark and arc, a high-temperature region, stretching from 2600 to 3000 K, is located at the center of the discharge channel, which can enhance the generations of the NO and NO_x [34, 35]. According to the Zeldovich mechanism, the gas temperature is around 2600 K, both the gas temperature and the vibrational temperature are in equilibrium, and the combination of heat and vibration promotes the formation of NO_x [35].

3.3. Influence of applied frequency

The discharge states can be changed by the applied frequency. Further, the generations of NO_x would be changed. In this section, we examined the discharge states and concentrations of NO, NO_2 and NO_x under different applied frequencies loaded on the discharge reactor. The experimental conditions are maintained as follows: the gas flow speed is 2.3 m/s (the gas flow state with laminar, as seen in table 1), the applied voltage is 8.0 kV, and the applied frequency is changed from 5.0 kHz to 9.0 kHz. Figures 9 and 10 show the characteristics of discharge states, discharge emission spectra, and NO_x. It was obtained that when the applied frequency is increased, the sliding arc discharge was transformed from arc discharge to spark discharge, meanwhile the NO, NO_2 and NO_x concentrations decreased, while the relative intensity of discharge emission increased.

Figure 9 shows that the discharge states changed with applied frequency. Figures 9(a)–(c) show that the discharge is arc discharge, transition state from arc to spark discharge, and spark discharge when the applied frequency is 5.0 kHz, 8.0 kHz, and 9.0 kHz, respectively.

This phenomenon can be understood as follows. With the increase of applied frequency, the discharge mode is changed from arc to spark. This is because the discharge reactor's structure that we designed approximates a coaxial capacitor when undischarged, and the high-voltage conductor connecting the reactor exhibits an inherent inductance. At lower frequencies, the current can swiftly charge the equivalent capacitor via the parasitic inductance of the high-voltage insulated conductor and precipitate dielectric breakdown and discharge. As a consequence, there is minimal change in reactor voltage, sustaining an arc discharge. However, at higher frequencies, the inductance hinders current flow, causing a quicker voltage drop upon breakdown, favoring spark discharge formation.

Figure 10 shows the intensities of discharge spectra and the concentrations of NO, NO_2 and NO_x at different applied frequencies. When the applied frequency is less than 8.0 kHz, the relative intensities of the discharge spectra present low level but the concentrations of NO, NO_2 and NO_x present large level. When the applied frequency increased, the relative intensities increased, and the concentrations of NO, NO_2 and NO_x decreased. When the applied frequency reached 9.0 kHz, the relative intensities of the discharge emission spectra increase to the largest, while the concentrations of NO, NO_2 and NO_x decrease to the lowest.

The results can be explained as follows. When the applied frequency is changed from 5.0 kHz to 9.0 kHz, the discharge state changes from arc discharge to spark discharge. Therefore, the relative intensities of discharge emission spectra are similar with figure 8. The concentrations of NO_x such as NO and NO_2 decreased slightly with frequency rise. Maybe it is because when the applied frequency is low, the discharge state is arc discharge, the discharge zone is abundant with charged particles, which are conducive to an accelerated discharge reaction rate. Conversely, at elevated applied frequencies typified by a spark discharge mode, conditions are favorable for the formation of NO. However, due to the ephemeral nature of the discharge, there are fewer charged particles in the discharge area, leading to a diminished discharge reaction rate, and a consequent reduction in NO concentration.

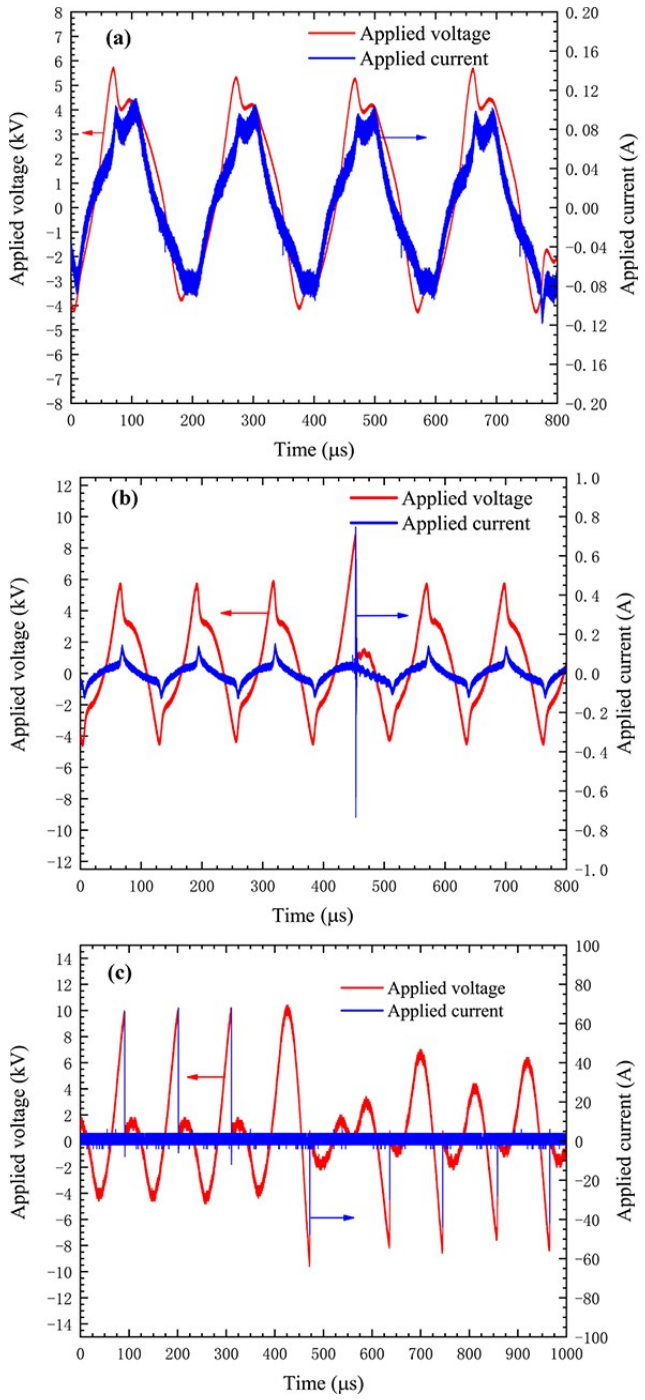

Figure 9. The waveforms of applied voltage and current at different applied frequencies. (a) Arc discharge under 5.0 kHz, (b) transition state from arc to spark under 8.0 kHz, (c) spark discharge under 9.0 kHz.

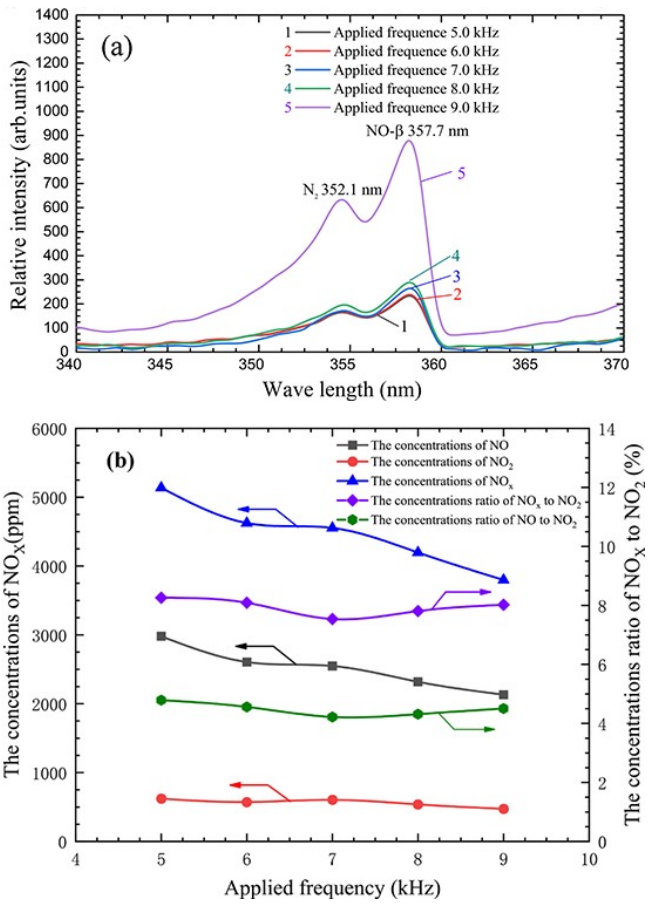

Figure 10. The relative intensities and the concentrations of NO_x under different applied frequencies. (a) The discharge emission spectral intensity, (b) the concentrations of NO, NO_2 and NO_x.

3.4. Reduction with molybdenum wire

The gas emissions contain a large amount of NO, NO_2 and O_2 at the tail of sliding arc discharge reactor. In order to reduce the NO_2 and O_2 from discharge reactor, the reduction property of molybdenum was employed to convert NO_2 to NO and react with O_2. The experimental conditions are maintained as follows: the gas flow speed is 2.3 m/s (with laminar, as seen in table 1), the applied voltage is 8.0 kV, the applied frequency is 7.0 kHz, and the discharge mode is keeping as sliding arc. The concentrations of NO, NO_2, and NO_x were evaluated by different diameters of molybdenum wire and operation temperatures.

The molybdenum wire diameters were selected as 0.1 mm and 0.5 mm, and the molybdenum wires were filled in the heating box and keeping 300 °C. Figure 11 shows the reduction characteristics. In figure 11(a), when we use a molybdenum wire with a diameter of 0.1 mm, the yields of NO and NO_x are higher than use the one of 0.5mm, and the concentration of NO_2 is smaller with the same conditions. In figure 11(b), when we use a molybdenum wire with a diameter of 0.1 mm, the concentration ratios of both NO versus NO_2 and NO_x versus NO_2 are larger than use the one of 0.5 mm.

The results can be explained as that the specific surface area of molybdenum wire affected the reduction reaction rate. Whereby the thin molybdenum wire with diameter of 0.1 mm has a larger specific surface area than the one with 0.5 mm, so the reaction rates on the surface with the diameter of 0.1 mm of molybdenum wire is higher than that with 0.5 mm. Consequently, the diameter of 0.1 mm of molybdenum wire is chosen for the subsequent experiment.

The reduction of molybdenum wire was examined from 25 °C to 400 °C. Figure 12 shows the concentrations of NO, NO_2 and NO_x and the ratios of NO and NO_x versus NO_2 at

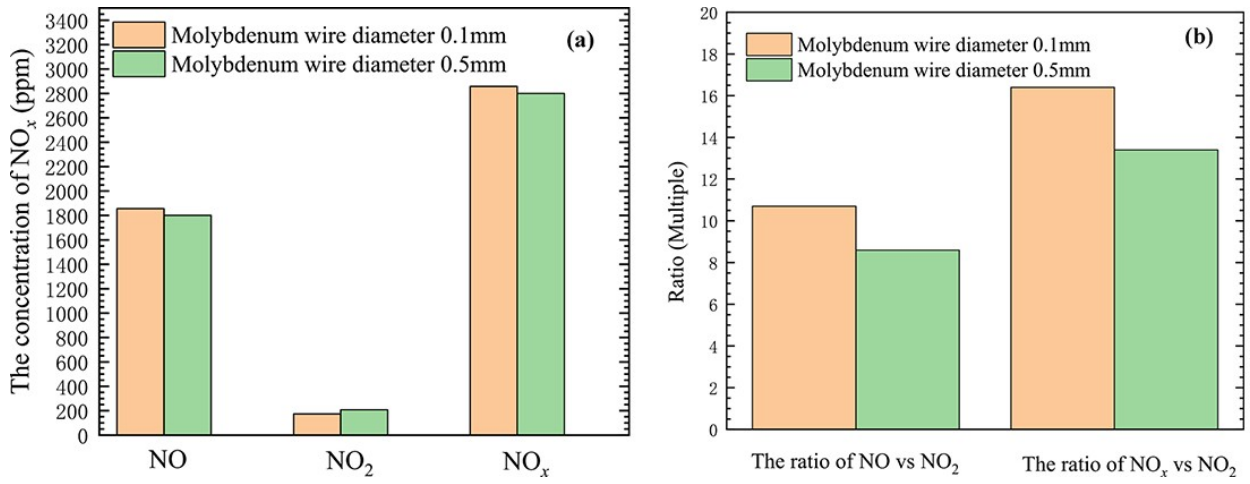

Figure 11. The molybdenum reduction under different wire diameters. (a) The concentrations of NO, NO_2 and NO_x, (b) the ratios of NO versus NO_2 and NO_x versus NO_2.

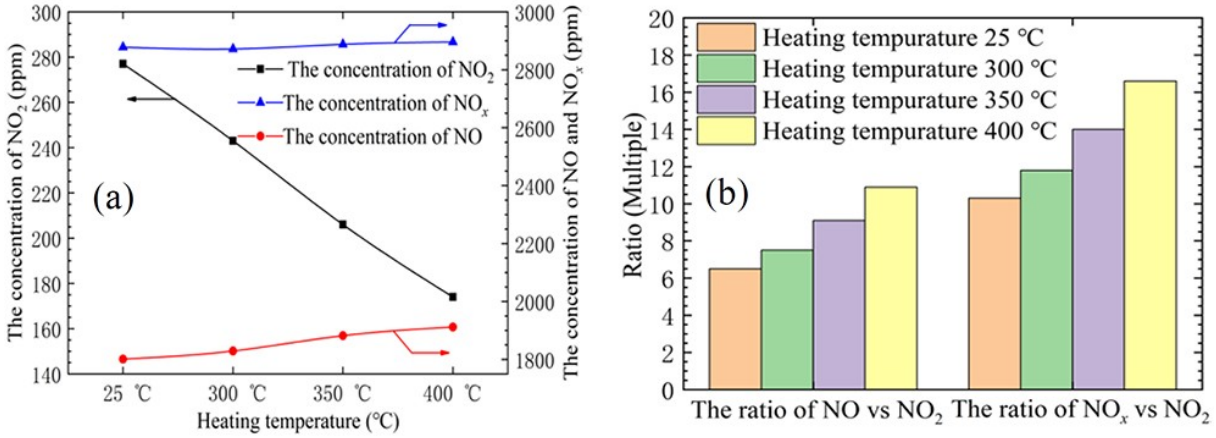

Figure 12. The molybdenum reduction under different temperatures. (a) The concentrations of NO, NO_2 and NO_x, (b) the ratios of NO versus NO_2 and NO_x versus NO_2.

different temperatures. Figure 12(a) shows that the concentrations of NO_2 decreased, and the concentrations of NO and NO_x increased with increasing temperature. Moreover, Figure 12(b) reveals a concurrent increase in the concentration ratios of both NO versus NO_2 and NO_x versus NO_2 with increasing temperature. This can be explained as the reduction reaction rate increases when the temperature increased, more reduction reaction happened between molybdenum wire and NO_2. As a result, more NO_2 was consumed, and more NO and NO_x were formed [32, 33]. The main reaction formulas are as follows [9]:

$$2NO_2 + Mo \rightarrow 2NO + MoO_2 \quad (16)$$

$$3NO_2 + Mo \rightarrow 3NO + MoO_3 \quad (17)$$

O_2 can also be removed by crossing the heated molybdenum wire as formulas:

$$O_2 + Mo \rightarrow MoO_2 \quad (18)$$

$$3O_2 + 2Mo \rightarrow 2MoO_3 \quad (19)$$

4. Conclusion

This work primarily investigates the impact of conical spiral rotary sliding arc discharge at different applied energies, applied frequencies, and air flow speeds on the concentrations of NO, NO_2, and NO_x, as well as the ratios of NO/NO_2 and NO_x/NO_2. The gas flow speeds in the discharge reactor can adjust the discharge mode from arc to spark, and the concentrations of NO, NO_2 and NO_x are closely related with discharge form. The applied frequency of high voltage loaded on the discharge reactor can change the discharge modes and concentrations of NO_x. Furthermore, the molybdenum reduction process can remove NO_2 and enhance NO and NO_x. This work provides experimental reference value for plasma synthesis of NO and plasma nitrogen fixation applications.

Acknowledgments

This work was partially supported by National Natural Science Foundation of China (No. 52477141), the Natural Science Foundation of the Jiangsu Province (No.

BK20191162), Fundamental Research Funds for the Central Universities (No. B210203006), the Research Fund of Innovation and Entrepreneurship Education Reform for Chinese Universities (No. 16CCJG01Z004), and Changzhou Science and Technology Program (No. CJ20190046).

References

[1] Jin J *et al* 2022 *Angew. Chem. Int. Ed.* **61** e202210980
[2] Peivastehgar H R *et al* 2023 *Expert Syst. Appl.* **230** 120704
[3] Vega Rasgado L A *et al* 2023 *Acta Pharm.* **73** 59
[4] Chen B *et al* 2021 *High Voltage Eng.* **47** 786 (in Chinese)
[5] Okamoto K *et al* 1998 *Chest* **114** 827
[6] Fadel P J 2017 *Hypertension* **69** 778
[7] Kukita I *et al* 1996 *J. Anesth.* **10** 44
[8] Gerlach H *et al* 2003 *Am. J. Respir. Crit. Care. Med.* **167** 1008
[9] Hu H *et al* 2007 *IEEE Trans. Plasma Sci.* **35** 619
[10] Yu B L *et al* 2015 *Sci. Transl. Med.* **7** 294ra107
[11] Li S R *et al* 2018 *Nitric Oxide* **73** 89
[12] Bruggeman P J *et al* 2021 *J. Appl. Phys.* **129** 200902
[13] Nayak G *et al* 2021 *Plasma Sources Sci. Technol.* **30** 115003
[14] Li Y D *et al* 2022 *J. Phys. D: Appl. Phys.* **55** 155204
[15] Tas M A, Van Hardeveld R and Van Veldhuizen E M 1997 *Plasma Chem. Plasma Process.* **17** 371
[16] Chen K *et al* 2022 *Plasma Sci. Technol.* **24** 044007
[17] Pawłat J *et al* 2019 *Plasma Chem. Plasma Process.* **39** 627
[18] Wandell R J *et al* 2019 *Plasma Chem. Plasma Process.* **39** 643
[19] Moldgy A *et al* 2020 *J. Phys. D: Appl. Phys.* **53** 434004
[20] Chen B Y *et al* 2016 *Plasma Sci. Technol.* **18** 278
[21] Chen B Y *et al* 2019 *J. Hazard. Mater.* **363** 55
[22] Ju R *et al* 2022 *J. Eng. Thermophys.* **43** 2225
[23] Shan M L *et al* 2019 *Plasma Sci. Technol.* **21** 074002
[24] Chen B Y *et al* 2019 *IEEE Trans. Plasma Sci.* **47** 837
[25] Kobayashi H *et al* 2019 *Proc. Combust. Inst.* **37** 109
[26] Feng R *et al* 2020 *Aerosp. Sci. Technol.* **99** 105752
[27] Zhang H *et al* 2016 *Plasma Sci. Technol.* **18** 473
[28] Ananthanarasimhan J *et al* 2019 *Plasma Sources Sci. Technol.* **28** 085012
[29] Choi S *et al* 2021 *Plasma Chem. Plasma Process.* **41** 1021
[30] Chen Z *et al* 2021 *J. Phys. D: Appl. Phys.* **54** 225203
[31] Guo L *et al* 2023 *Food Control* **148** 109662
[32] Huang P *et al* 2024 *Mar. Environ. Res.* **193** 106278
[33] Ašperger S 2003 *Chemical Kinetics and Inorganic Reaction Mechanisms* (New York: Springer)
[34] Li J C *et al* 2023 *Chem. Eng. J.* **478** 147483
[35] Jardali F *et al* 2021 *Green Chem.* **23** 1748